


An Overview of the Compton Scattering Calculation

Chen-Kai Qiao ^{*}, Jian-Wei Wei and Lin Chen

College of Science, Chongqing University of Technology, Chongqing 400054, China; redskywei@cqut.edu.cn (J.-W.W.); lchen@cqut.edu.cn (L.C.)

^{*} Correspondence: chenkaiqiao@cqut.edu.cn

Abstract: The Compton scattering process plays significant roles in atomic and molecular physics, condensed matter physics, nuclear physics and material science. It could provide useful information on the electromagnetic interaction between light and matter. Several aspects of many-body physics, such as electronic structures, electron momentum distributions, many-body interactions of bound electrons, etc., can be revealed by Compton scattering experiments. In this work, we give a review of ab initio calculation of Compton scattering process. Several approaches, including the free electron approximation (FEA), impulse approximation (IA), incoherent scattering function/incoherent scattering factor (ISF) and scattering matrix (SM) are focused on in this work. The main features and available ranges for these approaches are discussed. Furthermore, we also briefly introduce the databases and applications for Compton scattering.

Keywords: Compton scattering; bound electron; many-body interaction; ab initio approach



Citation: Qiao, C.-K.; Wei, J.-W.; Chen, L. An Overview of the Compton Scattering Calculation. *Crystals* **2021**, *11*, 525. <https://doi.org/10.3390/cryst11050525>

Academic Editors: Michal Ksawery Cyrański and Sławomir Grabowski

Received: 10 March 2021
Accepted: 6 May 2021
Published: 10 May 2021

Publisher's Note: MDPI stays neutral with regard to jurisdictional claims in published maps and institutional affiliations.



Copyright: © 2021 by the authors. Licensee MDPI, Basel, Switzerland. This article is an open access article distributed under the terms and conditions of the Creative Commons Attribution (CC BY) license (<https://creativecommons.org/licenses/by/4.0/>).

1. Introduction

The Compton scattering process is the scattering between a bound electron (e) in an atomic or molecular system and an incident photon (γ) in the electromagnetic field

$$e + \gamma \rightarrow e + \gamma'$$

It is one of the most important and mysterious electromagnetic processes in physics. This process was first noticed by A. H. Compton in 1923 [1,2], through which the quantum nature of X-rays was revealed successfully. Since Compton scattering was discovered in the 1920s, it has been carefully studied and extensively investigated for almost a century. The study of atomic Compton scattering could give us information on the interaction between light and matter, and it can also provide opportunities to reveal the underlying nature of electric structures, electron correlations, electron momentum distributions, and other aspects of physics [3–5]. Because of wide applications, Compton scattering is always an attractive topic in atomic physics, molecular physics, condensed matter physics, nuclear physics and material science [5–9] (Figure 1).

Since the 1920s, great efforts have been made to develop theoretical methods on ab initio calculations for the Compton scattering process. The simplest approach is the free electron approximation (FEA), which was first developed by O. Klein and Y. Nishina in 1929 [10]. In the FEA approach, the electrons in atomic or molecular systems are treated as free electrons. The atomic binding, electron shielding, electron correlations, electron motions around atomic nucleus, and other many-body effects are all omitted for simplicity. In FEA, the angular distribution for Compton scattering process is given by the Klein-Nishina formula [10,11]

$$\left(\frac{d\sigma}{d\Omega_f}\right)_{\text{FEA}} = \frac{r_0^2}{2} \left(\frac{\omega_C}{\omega_i}\right)^2 \left(\frac{\omega_i}{\omega_C} + \frac{\omega_C}{\omega_i} - \sin^2\theta\right) \quad (1)$$

Furthermore, in FEA approach, the final state photon energy ω_f after the scattering process is totally determined by the scattering angle θ in Compton scattering process

$$\omega_f = \omega_C = \frac{\omega_i}{1 + \omega_i(1 - \cos\theta)/m_e c^2} \quad (2)$$

Here, ω_C is known as the Compton energy. Because of computational simplicity and clear physical meaning, the FEA approach is most widely used in many branches of science. Over the past few decades, it has become a standard treatment for atomic Compton scattering in many textbooks. However, the FEA approach is much too simple, very little information on electronic structures and property of materials can be acquired. From Equation (1), it is evident that the angular distribution $(d\sigma/d\Omega_f)_{\text{FEA}}$ is independent of the electron momentum distributions in target materials.

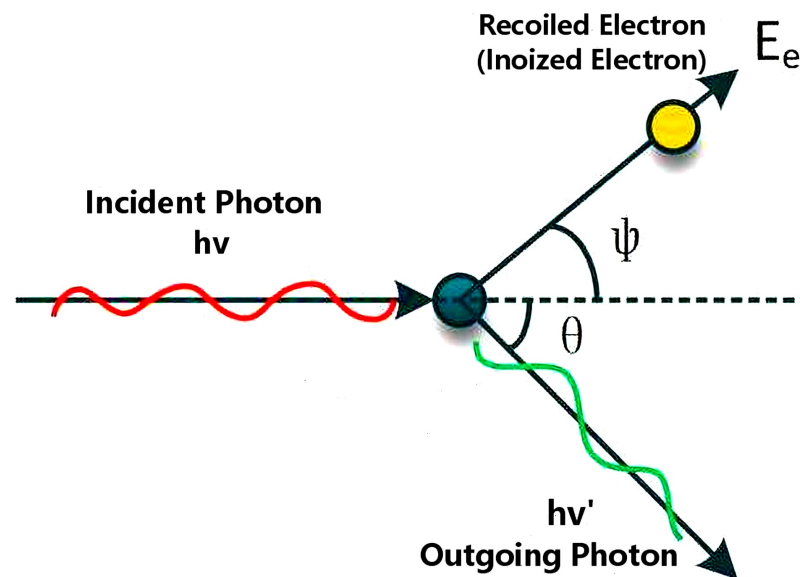


Figure 1. Schematic plot of Compton scattering process $e + \gamma \rightarrow e + \gamma'$.

Soon after the FEA approach was formulated by O. Klein and Y. Nishina in 1929, other approaches considering bound structures in atoms and molecules emerged. It was J. W. M. DuMond first realized that the atomic effects and electron motions would give inevitable effects on the scattering process. Then he introduced an approach to effectively include atomic binding effects as well as electron motion around atomic nuclei in the calculation of Compton scattering [12–14]. His approach was later known as the impulse approximation (IA). The DuMond's approach is the nonrelativistic impulse approximation (NRIA), and the same result was re-derived by P. Eisenberger et al. in the 1970s [15–18]. The relativistic impulse approximation (RIA) was developed until the 1970s–1980s by R. Ribberfors et al. [18–23]. In the IA formulation, the doubly differential cross-section (DDCS) for Compton scattering process can be factorized into two parts as follows:

$$\left(\frac{d^2\sigma}{d\omega_f d\Omega_f} \right)_{\text{IA}} = Y_{\text{IA}} \cdot J(p_z) \quad (3)$$

where Ω_f is the solid angle for final state outgoing photon. In Equation (3), Y_{IA} is a factor dependent on kinematical and dynamical properties of atomic Compton scattering, and irrelevant to the electronic structure of target materials. The factor $J(p_z)$, which is known as the Compton profile, is related to the momentum distributions of bound electrons in the atomic or molecular systems [24]. The Compton profile can reflect electronic structures, physical and chemical properties of target materials. It can be determined from theoretical calculations and experimental measurements. In actual ab initio calculations, the Compton profile $J(p_z)$ can be obtained using the nonrelativistic Hartree–Fock theory (HF), the relativistic Dirac–Hartree–Fock theory (DHF), and the density functional theory (DFT). It is

worth noting that in the IA approach, all the many-body effects in atomic and molecular systems in Compton scattering processes are incorporated into Compton profiles $J(p_z)$.

From the IA approach, the angular distribution of Compton scattering process can be obtained by integration of Equation (3), and the results is also a simple correction for FEA:

$$\left(\frac{d\sigma}{d\Omega_f}\right)_{\text{IA/ISF}} = \left(\frac{d\sigma}{d\Omega_f}\right)_{\text{FEA}} SF(\omega_i, \theta) \quad (4)$$

Here, $(d\sigma/d\Omega_f)_{\text{FEA}}$ is the angular distribution calculated in FEA approach as shown in Equation (1), and the correction factor $SF(\omega_i, \theta)$ is called the scattering function. It should be mentioned that apart from IA, there are other approaches which can give the same results in Equation (4). In other words, scattering function $SF(\omega_i, \theta)$ can also be calculated by other methods, such as the nonrelativistic Waller-Hartree theory [25,26]. This kind of approach, in which the angular distribution of Compton scattering is given by Equation (4), is called the incoherent scattering function or incoherent scattering factor (ISF) approach. Same as Compton profile $J(p_z)$, the scattering function $SF(\omega_i, \theta)$ can also reflect the electronic properties of target materials. On the one hand, $J(p_z)$ and $SF(\omega_i, \theta)$ can be measured from Compton scattering experiments with high precision. On the other hand, they can also be predicted by theoretical ab initio calculations in atomic, molecular, and condensed matter physics [24,27]. The Compton profile $J(p_z)$ and scattering function $SF(\omega_i, \theta)$ provide a bridge between Compton scattering and interdisciplinary studies in many branches of science. They can offer opportunities to learn the electronic structure and properties of target materials from Compton scattering process. Recently, there are many studies in which electronic structures and properties (include electron interactions, electron correlations, electron momentum distributions, band structures and fermi surfaces) are investigated through Compton profile and scattering function [6–9].

In recent decades, several methods beyond IA and ISF were emerged and formulated [28–34]. Among these approaches, the most successful one is based on the perturbation expansion of many-body electromagnetic interactions in atomic or molecular systems. In this approach, the DDCS of Compton scattering process can be calculated by the scattering matrix of a many-body theory

$$\left(\frac{d^2\sigma}{d\omega_f d\Omega_f}\right)_{\text{SM}} \propto |M_{if}|^2 \quad (5)$$

This approach is called the Scattering Matrix (SM) approach. In the SM, scattering matrix of Compton scattering process $M_{if} \propto \langle \Psi_f | H_I | \Psi_i \rangle$ can be calculated through the many-body interaction Hamiltonian H_I , which gives the many-body interaction between photon and bound electrons in atomic or molecular systems. The SM approach can take into account the factor of atomic bindings and electron interactions in atomic or molecular systems as much as possible. SM could handle with these many-body effects precisely in the dynamical process of Compton scattering. Recently, the SM formulation has revealed many nontrivial properties of Compton scattering, and it has attracted lots of interests in interdisciplinary studies [29,32].

Furthermore, there are several experiments which give supporting to the SM predictions [35–41]. Recently, Max Kircher et al. conducted a kinematically complete Compton scattering experiment using X-rays produced from accelerators with energy about 2.1 keV. By measuring the angular distribution of scattered photons, the experimental observations present large deviations with the FEA results. However, when SM approach is employed and ab initio numerical calculations are carried out, the experimental data are consistent with theoretical predictions [41]. These results indicate that the SM approach is becoming a promising tool to duel with Compton scattering with bound electrons, and it may have great impacts in this area in the near future.

This paper is organized as follows. Section 1 gives an introduction on Compton scattering and the development of theoretical methods on ab initio calculations of Compton scattering process. Section 2 gives a description of FEA, Section 3 discuss the IA approach,

and Section 4 is devoted to the ISF. The most advanced SM approach is presented in Section 5. Section 6 presents the comparisons between theoretical calculations and experimental measurements. Databases and applications for Compton scattering are briefly introduced in Section 7. Summaries are presented in Section 8.

2. Free Electron Approximation

In the free electron approximation (FEA), the electrons in Compton scattering are treated as free electrons, all the atomic binding effects and many-body interactions of bound electrons in atomic or molecular systems are neglected in the scattering process. Furthermore, it is also assumed that the bound electrons are at rest before the Compton scattering.

The FEA approach for Compton scattering process was given by O. Klein and Y. Nishina in 1929 [10]. In this formulation, the scattered photon energy ω_f in Compton scattering process is totally determined by its scattering angle θ via equation

$$\omega_f = \omega_C = \frac{\omega_i}{1 + \omega_i(1 - \cos\theta)/m_e c^2} \quad (6)$$

Here, m_e is the mass of electron, and ω_C is known as the Compton energy. When $\theta = 180^\circ$, the energy of scattered photon ω_f reaches its minimum, meanwhile the energy transfer $T = \omega_i - \omega_C$ arrives at its maximum. They can be expressed in the following

$$\omega_C^{\min} = \omega_f^{\min} = \frac{\omega_i}{1 + 2\omega_i/m_e c^2} \quad (7)$$

$$T^{\max} = \omega_i - \omega_C^{\min} = \omega_i - \frac{\omega_i}{1 + 2\omega_i/m_e c^2} \quad (8)$$

They correspond to the Compton edge of the Compton scattering spectrum of $d\sigma/dT$ [42,43].

In FEA formulation, the angular distribution of Compton scattering process is given by the Klein-Nishina formula [10,11]

$$\left(\frac{d\sigma}{d\Omega_f}\right)_{\text{FEA}} = \frac{r_0^2}{2} \left(\frac{\omega_C}{\omega_i}\right)^2 \left(\frac{\omega_i}{\omega_C} + \frac{\omega_C}{\omega_i} - \sin^2\theta\right) \quad (9)$$

and the corresponding DDCS can be expressed as

$$\left(\frac{d^2\sigma}{d\omega_f d\Omega_f}\right)_{\text{FEA}} = \frac{r_0^2}{4} \left(\frac{\omega_f}{\omega_i}\right)^2 \left[\frac{\omega_i}{\omega_f} + \frac{\omega_f}{\omega_i} + 4(\epsilon_i \cdot \epsilon_f)^2 - 2\right] \times \delta(\omega_f - \omega_C) \quad (10)$$

Here, r_0 is the classical radius of electron, ϵ_i and ϵ_f are polarization vectors for incoming and outgoing photons, ω_f and Ω_f are the energy and solid angle of the outgoing scattered photon, respectively. In the FEA results, due to the Dirac delta function $\delta(\omega_f - \omega_C)$ in Equation (10), the spectrum of DDCS is an isolated line located at Compton energy ω_C , which is known as "Compton line", as illustrated in Figure 2.

In the nonrelativistic limit, where the incoming photon energy $\omega_i \ll m_e c^2$, the angular distribution of Compton scattering reduced to

$$\left(\frac{d\sigma}{d\Omega_f}\right)_{\text{FEA}} = \frac{r_0^2}{2} \left(\frac{\omega_C}{\omega_i}\right)^2 (1 + \cos^2\theta) \quad (11)$$

In this case, the Compton energy becomes

$$\begin{aligned}\omega_f = \omega_C &= \frac{\omega_i}{1 + \omega_i(1 - \cos \theta)/m_e c^2} \\ &\approx \omega_i \left[1 - \frac{\omega_i}{m_e c^2} (1 - \cos \theta) \right] \\ &\approx \omega_i - \frac{K^2}{2m_e}\end{aligned}\quad (12)$$

where K is the momentum transfer in the Compton scattering process. Furthermore, in the elastic scattering limit $\omega_f = \omega_C \rightarrow \omega_i$ (namely the scattering angle $\theta \rightarrow 0$), the Equation (11) further reduce to the Thomson formula

$$\left(\frac{d\sigma}{d\Omega_f} \right)_{\text{Thomson}} = \frac{r_0^2}{2} (1 + \cos^2 \theta) \quad (13)$$

This is the differential cross-section of elastic scattering process between photon and free electron [11,24,27,44].

It should be mentioned that the Klein-Nishina formula in Equation (9) in FEA works well only in the cases that atomic binding energies are negligible, and the atomic electrons are approximately free. When the incident photon energy ω_i and energy transfer T are extremely high, the FEA result is appropriate. However, in many cases, the incident photon energy is comparable to the X-ray characteristic energies, in which the atomic bindings and electron many-body interactions cannot be neglected. Then the FEA formulation becomes invalid, and it fails to fit the experimental data [28].

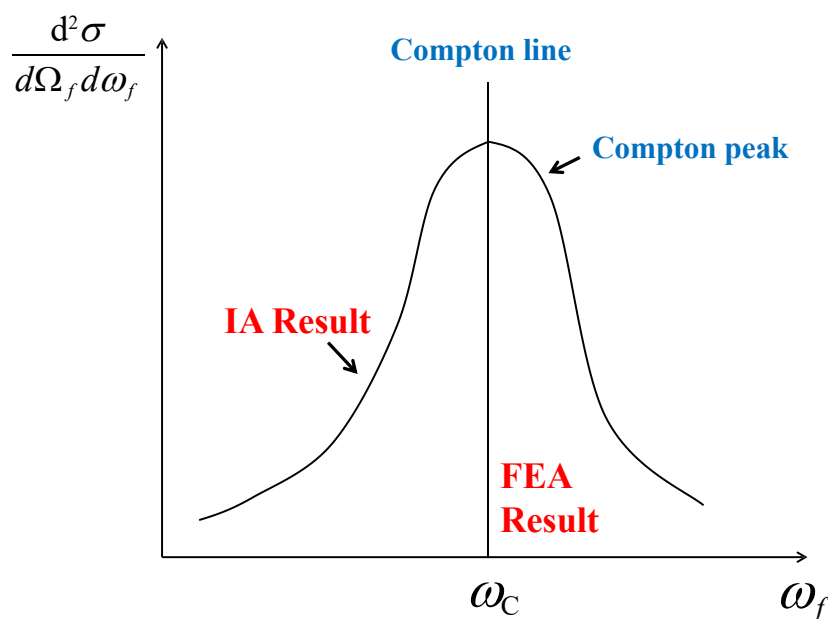


Figure 2. Schematic plot of the FEA and IA results of DDCS at scattering angle θ . The horizontal axis labels the final photon energy ω_f , and the vertical axis labels the DDCS of Compton scattering process.

3. Impulse Approximation

In the impulse approximation (IA) method, the atomic binding effects are effectively considered, and the electron pre-collision motions around atomic nuclei are also included. The basic starting point of IA approach can be shown in the following way. Because of atomic binding and electrons many-body interactions, the bound electrons in atomic and molecular systems have a momentum distribution $\rho(p)$ when moving around atomic or molecular nuclei. In principle, the momentum distribution for bound electrons is determined by ground state wavefunctions in atomic or molecular systems. In the Compton

scattering process, suppose electron in momentum eigenstate $|\mathbf{p}\rangle$ is scattered with incoming photon γ very rapidly, like an impulse acting on the electron. This scattering process is too quick to be disturbed by other electrons. In this way, electron momentum eigenstate $|\mathbf{p}\rangle$ scattered with incident photon γ independently as free electrons. Many-body interactions and interference terms between electrons with different momentum eigenstates ($|\mathbf{p}\rangle$ and $|\mathbf{p}'\rangle$) in the dynamical process of Compton scattering are omitted for simplicity. Therefore, the DDCS of the Compton scattering process is achieved through a summation of the scattering probability for all possible momentum eigenstates

$$\left(\frac{d^2\sigma}{d\omega_f d\Omega_f}\right)_{\text{IA}} = \iiint d^3p \rho(\mathbf{p}) \left(\frac{d^2\sigma(\mathbf{p})}{d\omega_f d\Omega_f}\right)_{\text{FEA}} \times \delta(E_i + \omega_i - E_f - \omega_f) \quad (14)$$

In this expression, $(d^2\sigma(\mathbf{p})/d\omega_f d\Omega_f)_{\text{FEA}}$ is the DDCS of Compton scattering between photon γ and electron in momentum eigenstate $|\mathbf{p}\rangle$, which can be calculated by FEA. The E_i and E_f are the energies of electron before and after Compton scattering process. The Equation (14) can be viewed as the basic starting point of IA approach, and different versions of IA treatments are achieved by applying different numerical schemes in calculating Equation (14) [42].

The aforementioned atomic binding effects and electron pre-collision motion make the IA results significantly different from FEA results. In the FEA results, there is a one-to-one correspondence between the final state photon energy ω_f and the scattering angle θ (see Equation (6)). In the IA approach, due to the electron motion around atomic nuclei, the energy of the scattered photon ω_f cannot be totally determined by its scattering angle θ as in FEA. For the same scattering angle θ , the outgoing photon energy ω_f has a continuous distribution. The maximum cross-section is located at the Compton energy ω_C , which is given by Equation (6), forming a “Compton peak” in the spectrum of DDCS. In Figure 2, the DDCS of Compton scattering predicted in FEA and IA approaches are illustrated schematically. Sometimes, it is more enlightening to interpret the emergence of “Compton peak” as the Doppler broadening effect of the “Compton line” (located at Compton energy ω_C) [45,46]. This Doppler effect is due to the bound electrons’ motion around atomic nuclei.

The nonrelativistic impulse approximation (NRIA) was first developed by DuMond in the 1930s [12–14]. In the 1970s, Eisenberger and Platzman re-derived the NRIA formulation based on the more accurate scattering matrix (SM) approach. It is shown that NRIA can be viewed as the leading order approximation of SM approach [15–18]. In NRIA, the DDCS of Compton scattering is given by [14,15]

$$\begin{aligned} \left(\frac{d^2\sigma}{d\omega_f d\Omega_f}\right)_{\text{NRIA}} &= \frac{r_0^2 m_e \omega_f}{2 K \omega_i} (1 + \cos^2 \theta) J(p_z) \\ &= Y_{\text{NRIA}} \cdot J(p_z) \end{aligned} \quad (15)$$

Here, K is the modulus of the momentum transfer vector $\mathbf{K} \equiv \mathbf{k}_f - \mathbf{k}_i$ in Compton scattering process, and p_z is given by

$$p_z = \frac{K}{2} - \frac{m_e(\omega_i - \omega_f)}{K} \quad (16)$$

In Equation (15), the factor $Y_{\text{NRIA}} = r_0^2 m_e \omega_f (1 + \cos^2 \theta) / 2K\omega_i$ relies on the dynamical and kinematical properties of Compton scattering process in the nonrelativistic limit. The $J(p_z)$ is a factor coming from the many-body effects in atomic or molecular systems, which is known as the “Compton profile” [24]

$$J(p_z) \equiv \iint \rho(\mathbf{p}) dp_x dp_y \quad (17)$$

where $\rho(\mathbf{p})$ is the electron momentum density of the atomic or molecular ground-states. The Compton profile is closely related to the electronic properties of the atomic or molecular systems, and it has been widely studied in atomic, molecular and condensed matter

physics [6,7,9]. Furthermore, for most of the atomic systems, the momentum distribution is spherical symmetric, then the Compton profile reduces to

$$J(p_z) = 2\pi \int_{|p_z|}^{\infty} p\rho(p)dp \quad (18)$$

In these cases, the Compton profile $J(p_z)$ is bell-shaped and axisymmetric around the $p_z = 0$ axis. However, many of the molecular or condensed matter systems do not have this spherical symmetric property.

The relativistic impulse approximation (RIA) was developed by R. Ribberfors et al. in 1975–1985 [18–23]. In this formulation, the DDCS of Compton scattering is given by [21,22,47]

$$\begin{aligned} \left(\frac{d^2\sigma}{d\omega_f d\Omega_f} \right)_{\text{RIA}} &= \frac{r_0^2 m_e m_e c^2}{2 K E(p_z)} \frac{\omega_f}{\omega_i} \bar{X}(p_z) J(p_z) \\ &= Y_{\text{NRIA}} \cdot J(p_z) \end{aligned} \quad (19)$$

The same as in NRIA, $Y_{\text{RIA}} = r_0^2 m_e^2 c^2 \omega_f \bar{X}(p_z) / 2K\omega_i E(p_z)$ is a factor depends on kinematical and dynamical properties of Compton scattering. The factor relevant to atomic or molecular structure is the Compton profile $J(p_z)$ defined in Equation (17). In Equation (19), K is the modulus of the momentum transfer vector $\mathbf{K} \equiv \mathbf{k}_f - \mathbf{k}_i$ and p_z is the projection of the electron's initial momentum on the momentum transfer direction

$$p_z = \frac{\mathbf{p} \cdot \mathbf{K}}{K} = \frac{\omega_i \omega_f (1 - \cos \theta) - E(p_z)(\omega_i - \omega_f)}{c^2 K} \quad (20)$$

Moreover, the function $\bar{X}(p_z)$ is defined to be

$$\bar{X}(p_z) = \frac{K_i(p_z)}{K_f(p_z)} + \frac{K_f(p_z)}{K_i(p_z)} + 2m_e^2 c^2 \left(\frac{1}{K_i(p_z)} - \frac{1}{K_f(p_z)} \right) + m_e^4 c^4 \left(\frac{1}{K_i(p_z)} - \frac{1}{K_f(p_z)} \right)^2 \quad (21)$$

with K_i and K_f defined as

$$K_i(p_z) = \frac{\omega_i E(p_z)}{c^2} + \frac{\omega_i(\omega_i - \omega_f \cos \theta)p_z}{c^2 q} \quad (22)$$

$$K_f(p_z) = K_i(p_z) - \frac{\omega_i \omega_f (1 - \cos \theta)}{c^2} \quad (23)$$

$$E(p_z) = \sqrt{m_e^2 c^4 + p_z^2 c^2} \quad (24)$$

To summarize, combining Equations (15) and (19), it is clear that the DDCS of Compton scattering process calculated in IA approach factorizes into two parts

$$\left(\frac{d^2\sigma}{d\omega_f d\Omega_f} \right)_{\text{IA}} = Y_{\text{IA}} \cdot J(p_z) \quad (25)$$

where Y_{IA} is a factor dependent on kinematical and dynamical properties of Compton scattering process, and the Compton profile $J(p_z)$ is relevant to the electron momentum distribution of the atomic or molecular ground-states. It is worth noting that in the IA approach, all the many-body effects in atomic and molecular systems in Compton scattering process are incorporated into Compton profiles $J(p_z)$. The Compton profile can reflect electronic structures and properties of target materials. Therefore, it provides us an opportunity to learn the electronic structures, electron interactions and properties of materials from Compton scattering processes. In actual ab initio calculations, the Compton profile $J(p_z)$ can be calculated by the nonrelativistic Hartree–Fock theory (HF), the relativistic Dirac–Hartree–Fock theory (DHF), and the density functional theory

(DFT) [24,48–53]. Interestingly, the FEA result can be simply reduced from IA result by replacing the Compton profile with the Dirac delta distribution $J(p_z) = \delta(p_z)$. Considering the atomic binding effects and electron pre-collision motions, the IA formulation could overcome the shortcomings in the FEA method. It is a practical approach to calculate the Compton scattering of bound electrons with X-rays and gamma-rays. Later research shows that the IA approach could serve as a good approximation in energy region near the “Compton peak” [29,42] (see Figures 2 and 3).

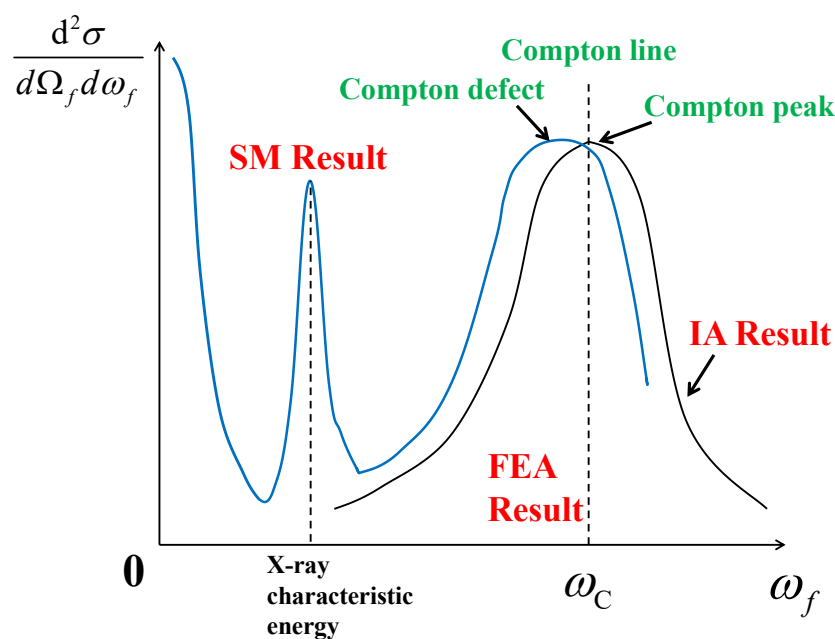


Figure 3. Schematic plot of Compton scattering DDCS in the SM approach at the scattering angle θ . The horizontal axis labels the final photon energy ω_f , and the vertical axis labels the DDCS of Compton scattering process.

Although the IA formulation effectively takes into consideration the atomic binding effects and electron pre-collision motions around atomic nuclei, it still has limitations in dealing with Compton scattering. In IA formulation, all the many-body effects in Compton scattering process are incorporated into Compton profile $J(p_z)$, which is an observable only related to the atomic or molecular ground-states. The many-body effects coming from the ionized states and the interference terms among different momentum eigenstates are still insufficient in the dynamical process of Compton scattering. In the past few years, several approaches beyond the IA had already been investigated [28–34]. This research, which mainly employs the low-energy theorem (LET) and scattering matrix (SM) approaches, has revealed many nontrivial properties of Compton scattering and has attracted lots of interests in interdisciplinary studies. Through comparing IA with these more advanced approaches, it is clear that the validity region for IA approach is just near the Compton peak region. Furthermore, in the validity region of IA, the momentum transfer K in Compton scattering is much larger than the average momentum p_{average} for bound electrons (namely $p_{\text{average}}/K \ll 1$) [28,32,54,55]. We will specialize in the SM approach in Section 5.

4. Incoherent Scattering Factor/Incoherent Scattering Function

In this section, we give an introduction of the incoherent scattering function/incoherent scattering factor (ISF) approach. First, we can use the IA result as an example to illustrate the ISF approach. Starting from the IA result of DDCS in Equations (15) and (19), the angular distribution of Compton scattering can be calculated by an integration of final state photon energy ω_f over the allowed range

$$\frac{d\sigma}{d\Omega_f} = \int_{\omega_{\min}}^{\omega_{\max}} \frac{d^2\sigma}{d\omega_f d\Omega_f} d\omega_f \quad (26)$$

After this integration, the angular distribution $d\sigma/d\Omega_f$ can be reduced to the product of Klein-Nishina result in Equation (9) and a correction factor [21,22].

$$\left(\frac{d\sigma}{d\Omega_f}\right)_{\text{IA/ISF}} = \left(\frac{d\sigma}{d\Omega_f}\right)_{\text{FEA}} SF(\omega_i, \theta) \quad (27)$$

The correction factor $SF(\omega_i, \theta)$ is called the scattering function or scattering factor. Apart from IA, there are other ways to give the same results in Equation (27) [25,26]. This kind of approach, in which the angular distribution of Compton scattering is given by Equation (27) and $SF(\omega_i, \theta)$, is called the ISF approach.

We can use the following way to understand the physical meaning of scattering function $SF(\omega_i, \theta)$. If the atomic or molecular system has N electrons, and each electron scattered with photon independently as free electrons. Then the angular distribution of Compton scattering for whose system becomes

$$\left(\frac{d\sigma}{d\Omega_f}\right)_{\text{FEA}}^{\text{total system}} = N \left(\frac{d\sigma}{d\Omega_f}\right)_{\text{FEA}}^{\text{single electron}} \quad (28)$$

Therefore, the scattering function $SF(\omega_i, \theta)$, which is defined to be the ratio between the contribution of total system and that of single electron

$$SF(\omega_i, \theta) \equiv \frac{\left(\frac{d\sigma}{d\Omega_f}\right)_{\text{FEA}}^{\text{total system}}}{\left(\frac{d\sigma}{d\Omega_f}\right)_{\text{FEA}}^{\text{single electron}}} \quad (29)$$

can be view as the number of activated electrons in the Compton scattering process.

Here, we would present the scattering function $SF(\omega_i, \theta)$ calculated within the RIA approach, the scattering function calculated using NRIA can be obtained in a similar way. To obtain scattering function $SF(\omega_i, \theta)$ from RIA, we need to substitute the DDCCS in Equation (19) into Equation (26) and evaluate the integral. After using some approximations, the factorization results of angular distribution in Equation (27) can be obtained. Finally, the scattering function $SF(\omega_i, \theta)$ can be expressed as [21,47,56]:

$$SF(\omega_i, \theta) = \sum_i Z_i \Theta(\omega_i - U_i) n_i(p_i^{\max}) \quad (30)$$

The Heaviside step function $\Theta(\omega_i - U_i)$ guarantees that only the activated electrons are included. In Compton scattering process, the electron becomes activated when the transferred energy $T = \omega_i - \omega_f$ is larger than the binding energy U_i for i -th subshell. In Equation (30), Z_i is the number of electrons in i -th subshell, p_i^{\max} denotes the maximum value of p_z for the i -th subshell electron

$$p_i^{\max} = \frac{\omega_i(\omega_i - U_i)(1 - \cos\theta) - m_e c^2 U_i}{c \sqrt{2\omega_i(\omega_i - U_i)(1 - \cos\theta) + U_i^2}} \quad (31)$$

and function $n_i(p_i^{\max})$ is defined to be an integral for Compton profile

$$n_i(p_i^{\max}) = \int_{-\infty}^{p_i^{\max}} J_i(p_z) dp_z \quad (32)$$

Here, the function $J_i(p_z)$ is the single-electron Compton profile for i -th subshell. It can be expressed as

$$J_i(p_z) = \iint \rho_i(\mathbf{p}) dp_x dp_y \quad (33)$$

The $\rho_i(p_z)$ is the electron momentum distribution for i -th subshell, which can be calculated by ground state momentum wavefunctions. Then the total Compton profile for atomic or molecular system is given by

$$J(p_z) = \sum_i Z_i J_i(p_z) \quad (34)$$

The quantity $SF(\omega_i, \theta)$ in Equation (30) is the scattering function in RIA formulation. In principle, it is a two-variable function depending on initial photon energy ω_i and scattering angle θ . However, in the nonrelativistic limit, these two variables are related to each other and they cannot be fully separated, which makes the scattering function $SF(\omega_i, \theta)$ further reduce to a single-variable function [27,56]. The interdependence of ω_i and θ is realized via a new variable x used in Hubbell's work [27]

$$x[\text{\AA}^{-1}] = \sin\left(\frac{\theta}{2}\right)/\lambda[\text{\AA}] \quad (35)$$

$$\lambda[\text{\AA}] = \frac{12.3984}{\omega_i[\text{keV}]} \quad (36)$$

Actually, in this expression, x is proportional to the momentum transfer in the elastic scattering between photon and electron, which is the Rayleigh scattering process, at scattering angle θ .

It should be mentioned that although the above ISF result on angular distribution displayed in Equation (27) is derived from IA approach, the same result can be derived from other theories. In other words, there are alternative methods to calculate the scattering function $SF(\omega_i, \theta)$ in Compton scattering process. For instance, in the nonrelativistic Waller–Hartree theory, the scattering function is given by [25]

$$SF(K, N)_{\text{WH}} = N - \sum_{i=1}^N f_{ii}(K) - \sum_{i=1}^N \sum_{j=1}^N |f_{ij}(K)|^2 \quad (37)$$

where N is the number of electrons in atomic or molecular systems, and $f_{ij}(K, N)$ is form factor

$$f_{ij}(K) = \iiint \psi_i^*(\mathbf{r}) e^{i\mathbf{K}\cdot\mathbf{r}} \psi_j(\mathbf{r}) d\mathbf{r} \quad (38)$$

Here, $\psi(\mathbf{r})$ is the single-electron wavefunction for i -th electron, and $\mathbf{K} \equiv \mathbf{k}_f - \mathbf{k}_i$ is momentum transfer vector. Later, in a work presented by J. H. Hubbell et al., a more accurate expression for scattering function was used to include ionized state effects [27]

$$SF(K, N) = \left\langle \Psi \left| \sum_{i=1}^N \sum_{j=1}^N e^{i\mathbf{K}\cdot(\mathbf{r}_i - \mathbf{r}_j)} \right| \Psi \right\rangle - [F(K, N)]^2 \quad (39)$$

where the summation is over all electrons in atomic or molecular systems. In this equation, $|\Psi\rangle$ is the ground state for atomic or molecular systems, \mathbf{r}_i and \mathbf{r}_j are position vectors for i -th and j -th electrons correspondingly, and $F(K, N)$ is the total form factor for atoms or molecules defined by

$$F(K, N) = \int \rho(r) e^{i\mathbf{K}\cdot\mathbf{r}} d\mathbf{r} \quad (40)$$

The above results predicted by ISF approach are valid when variable x and momentum transfer K are large, which has been confirmed by experiments [36,39,57]. However, there are limitations on the ISF approach. First, the ISF approach based on Equation (27) can only be used to calculate the angular distribution for Compton scattering process. The information coming from the more differential quantities, such as DDCS $d^2\sigma/d\omega_f d\Omega_f$, are lost in the integration. Secondly, in the ab initio calculations of scattering function $SF(\omega_i, \theta)$, contributions from Compton scattering and Raman scattering cannot be efficiently distin-

guished [29,40]. In numerical tabulations, contributions of these two processes are summed over to give a total result. In the high energy region, it is lucky the Compton scattering is dominant compared to the Raman scattering.

The same as Compton profile $J(p_z)$ discussed in Section 3, the scattering function $SF(\omega_i, \theta)$ could also reflect the properties of target materials. Therefore, scattering function also creates a bridge between Compton scattering and interdisciplinary studies. It offers opportunities to learn the electronic structure and properties of target materials from Compton scattering process [27,57].

5. Scattering Matrix Approach

In this section, we specialize in the scattering matrix (SM) approach. In this approach, atomic binding effects and many-body effects in atomic or molecular systems are taken into account more precisely. It not only provides us a more complete understanding of the main features of Compton scattering with bound electrons, but also helps us recognize the validity regions for other methods (such as FEA and IA). With these advantages, the SM approach has attracted large interests in interdisciplinary studies [32,34].

In the SM approach, the DDCS of Compton scattering process can be calculated by the scattering matrix of a many-body theory

$$\left(\frac{d^2\sigma}{d\omega_f d\Omega_f} \right)_{SM} \propto |M_{if}|^2 \quad (41)$$

Therefore, it is known as the scattering matrix (SM) approach. In this approach, the scattering matrix of Compton scattering process $M_{if} \propto \langle \Psi_f | H_I | \Psi_i \rangle$ can be calculated through the many-body interaction Hamiltonian H_I for atomic or molecular systems. The interaction Hamiltonian H_I is determined by electromagnetic interactions between bound electrons and radiation photon fields, and it is given by the Quantum Electrodynamics (QED) for atomic and molecular systems. There are two categories of SM approaches: the nonrelativistic and relativistic theories. In the nonrelativistic theories, the interaction Hamiltonian H_I is expressed as

$$H_I^{\text{nonrelativistic}} = \sum_{i=1}^N \left[\frac{e^2}{2m_e c} A^2 - \frac{e}{m_e c} \mathbf{p}_i \cdot \mathbf{A} \right] \quad (42)$$

Here, \mathbf{A} is quantized electromagnetic vector potential which describe radiation field of incoming photon acting on atomic or molecular system. The \mathbf{p}_i is the momentum for i -th electron, and the summation is over all electrons. In the relativistic theories, the interaction Hamiltonian is written by

$$H_I^{\text{relativistic}} = - \sum_{i=1}^N c \boldsymbol{\alpha}_i \cdot \mathbf{A} \quad (43)$$

where $\boldsymbol{\alpha}_i$ is the conventional Dirac matrices for i -th electrons.

The earlier works on SM approach were carried out based on the nonrelativistic Hamiltonian H_I , and they were restricted to A^2 term (only the first term in the square bracket of Equation (42) was included) [15,58–60]. The contributions from the second term $\mathbf{p}_i \cdot \mathbf{A}$ were accomplished by M. Gavrilu et al. in the 1970s [61–64]. The full relativistic treatment was first attempted by I. B. Whittingham [65,66] and then developed by P. M. Bergstrom, T. Surić, R. H. Pratt et al. in the 1990s [28,29,54,67,68]. In these works, the initial and final states ($|\Psi_i\rangle$ and $|\Psi_f\rangle$) in atomic or molecular systems were calculated within the independent particle model (IPM), in which the single-electron states are solved through the unperturbed Hamiltonian

$$H_0 = \frac{\mathbf{p}_i^2}{2m_e} + U(\mathbf{r}_i) \quad (44)$$

Here, p_i and r_i are the momentum and position of the i -th electron. In the IPM method, the potential for i -th electron $U(r_i)$ is given by the mean field of atomic nuclear potential and many-body interactions from other bound electrons. The IPM treatment may not be a perfect method in dueling with electron non-local exchange and correlations, and new treatments to tame electron non-local exchange in the framework of SM is still in development [40]. With the initial and final state wavefunctions $|\Psi_i\rangle$, $|\Psi_f\rangle$, and interaction Hamiltonian H_I , the DDSCS of Compton scattering process can be achieved from Equation (41). There are a lot of techniques to calculate the matrix elements M_{if} in Equation (41), which is beyond the scope of this work. In particular, in the nonrelativistic theories, the scattering matrix element $M_{if} \propto \langle \Psi_f | H_I | \Psi_i \rangle$ reduces to the Kramers–Heisenberg–Waller (KHW) matrix element [69–71].

The spectrum of DDSCS in Compton scattering obtained from SM approach has three main features. First, when final state photon energy approach to zero, namely in the $\omega_f \rightarrow 0$ limit, an infrared rise emerges in the spectrum [32]. This infrared rise is an example of infrared divergence behavior, which is a common feature of QED [11,72]. The same infrared rise behavior is also predicted in the low-energy theorem (LET) method [73,74] (Infrared behavior arises in the $\omega_f \rightarrow 0$ limit, and the energy transfer $T = \omega_i - \omega_f \rightarrow \omega_i$). In these cases, the energy of outgoing photons is tiny, and it makes these outgoing photons very difficult to observe experimentally. The Compton scattering process is happened as if the incident photon energy ω_i is totally absorbed by atomic or molecular systems without producing notable influences, similar to the photoionization process/photoelectric effect). Secondly, some resonant peaks appear near the characteristic X-rays energies, which are the transition energies between different atomic or molecular states (When the resonant peaks emerge at X-ray characteristic energies, the electron undergoes a deexcitation process to lower energy intermediate states before it is ionized in Compton scattering process. The resonant peak energies correspond to the transition energies in these deexcitation subprocesses). This resonant behavior mostly come from Compton scattering with L and M shell electrons [29]. At last, the “Compton peak” is reproduced in the vicinity of Compton energy ω_C . In the SM results, the center of Compton peak $\omega_{\text{cen}}^{\text{SM}}$ is slightly different from the Compton energy ω_C , and the difference $\delta = \omega_{\text{cen}}^{\text{SM}} - \omega_C$ leads to the “Compton defect” or “asymmetry of Compton profile” [32,40,75] (There are other ways to define “asymmetry of Compton profile”. For instance, in reference [75], the “asymmetry of Compton profile” is defined as $A = \frac{J(p_z, K) - J(-p_z, K)}{J(p_z=0, K)}$. Here, K is the modulus of momentum

transfer vector $K \equiv k_f - k_i$ in Compton scattering process, and $J(p_z, K) = \frac{(d^2\sigma/d\Omega_f d\omega_f)_{\text{SM}}}{Y_{\text{IA}}}$ is the effective Compton profile extracted from SM results. Actually, from a detailed analysis of kinematical behavior in Compton scattering process, the following conclusions can be obtained. If the summit of Compton peak in the SM result is located at Compton energy ω_C exactly, namely $\delta = \omega_{\text{cen}}^{\text{SM}} - \omega_C = 0$, the extracted Compton profile $J(p_z, K)$ would reach its maximum value at $p_z = 0$. In this case, $J(p_z, K)$ is axisymmetric around $p_z = 0$ for spherical symmetric atoms, the same as conventional Compton profile in Equation (18), and there is no “asymmetry”. However, when the summit of Compton peak is shifted from Compton energy ω_C , $J(p_z, K)$ would not produce the maximal value at $p_z = 0$. In this case, $J(p_z, K)$ is not axisymmetric around $p_z = 0$ for spherical symmetric atoms, so there is asymmetry in $J(p_z, K)$ between positive and negative p_z values). When the modulus of momentum transfer K in Compton scattering is sufficiently large such that inequalities $p_{\text{average}}/K \ll 1$ and $a/K \ll 1$ are satisfied, the “Compton defect” becomes extremely small and it can be neglected [28,29,32,54,68,75]. Here, p_{average} is the average momentum in atomic or molecular systems, a is parameter defined to be $a = m_e c Z \alpha$, and $\alpha \approx 1/137$ is the fine-structure constant. In these cases, the RIA result does not present notable deviations from the SM result in the Compton peak region. The spectrum of DDSCS predicted by SM result is illustrated in Figure 3. To summarize, in the SM results, DDSCS of Compton scattering exhibit infrared rise, the resonant peak, and the Compton peak. The three categories of peaks arise in different energy ranges. When we discuss the Compton peak, the final photon energy ω_f should near Compton energy ω_C , and the

incident photon energy $\omega_i > \omega_C$. When the resonant peak is observed, final photon energy ω_f is just near the X-ray characteristic energy of atoms or molecules, and initial photon energy ω_i is usually much larger than this characteristic energy. To see the infrared rise, final photon energy ω_f should go to zero (namely $\omega_f \rightarrow 0$), while the incident energy ω_i is not necessary to be very small.

It should be noted that the SM approach is still in development now [32–34,37,38,40,76–78]. In some studies, new treatments and techniques are pursued to handle electron non-local exchange and correlation by methods beyond IPM [37,38,76]. Other studies are devoted to more complex scattering process, for instance, Hopersky et al. investigated the Compton scattering and Rayleigh scattering of two X-ray photons [77,78]. Apart from the theoretical explorations, there are several experiments which have provided evidence to confirm the SM approach [35–41]. Recently, Max Kircher et al. conducted a kinematically complete Compton scattering experiment using X-rays produced from accelerators with energy about 2.1 keV. By measuring the angular distribution of the scattered photon, the experimental observations present large deviations with the FEA results, but the experimental data are consistent with theoretical predictions from SM approach [41]. This observation indicates that the SM approach is becoming a promising tool to duel with Compton scattering with bound electrons. Furthermore, the resonant peaks in Compton spectrum near the characteristic X-rays energies predicted by SM approach have also been confirmed by experiments [35]. However, despite lots of attempts, the infrared rise behavior in Compton spectrum predicted by SM approach (which is also predicted by LET approach) has not been confirmed in experiments yet.

Although there is still inadequacy in duel with some many-body effects (such as the electron non-local exchange), the SM is the most advanced and accurate approach in the ab initio calculations of Compton scattering with bound electrons over recent years. First, in SM approach, the initial state $|\Psi_i\rangle$, final state $|\Psi_f\rangle$, and the dynamical process of Compton scattering are all treated by many-body QED theory of atomic or molecular systems. It is a fully quantum many-body approach, not just making simple corrections to the FEA results, as with RIA and ISF approaches. Second, the SM approach can take the many-body effects in atomic or molecular systems into account as much as possible. In this approach, atomic bindings, electron motions around atomic nuclei and electron many-body interactions are all considered in the starting points of theoretical treatments. Third, SM results can reflect all the main features in Compton scattering process: the infrared rise at low energy, the resonant peak at X-ray characteristic energy, and the broaden “Compton peak” near the Compton energy ω_C . With the aforementioned superiority, SM can make more accurate predictions in the entire region of the spectrum. Furthermore, many other approaches, such as FEA and IA, can be derived from the SM approach by making appropriate and simplified approximations. Since it was developed, SM have attracted lots of interests in atomic and molecular physics, and it may have great impacts in these areas in the near future.

6. Comparisons between Theoretical Calculations and Experimental Measurements

In the section, to have a better understanding of characteristics and limitations of the approaches described above, the comparisons between theoretical calculations and experimental measurements are provided. Limited by the scope of this work, only a few representative examples are presented. For more examples, the readers can resort to references [28,36,57,79–85].

For the angular distribution of Compton scattering process, the theoretical and experimental results of Fe and Cu are presented in Figure 4. In this figure, the incident photon energy is $\omega_i = 59.5$ keV. We choose Fe and Cu elements as representative examples of elemental metal and ferromagnetic metal, respectively. Results of other elements exhibit a similar behavior, and they are not displayed in this figure. The readers could find more examples in references [79–82]. The experimental measurements from references [80,81] and the theoretical predictions of FEA and ISF approaches [81,82] are plotted in this figure. In reference [82], the scattering function $SF(\omega_i, \theta)$ is calculated using Equation (30) in RIA

framework [81,82] (Please note that in Section 4, we have mentioned that the scattering function $SF(\omega_i, \theta)$ can be obtained from RIA, Waller-Hartree theory, and other methods. In particular, within the RIA framework, the scattering function $SF(\omega_i, \theta)$ is calculated through the integration of Compton profile $J(p_z)$, see Equations (30)–(33)). The results in Figure 4 indicate that ISF is a better approach than FEA in calculating the angular distribution for Compton scattering process. The ISF results successfully reproduce experimental measurements at all angles, while the FEA results can bring about large discrepancies in the small angle regions. In this region, both the energy transfer and momentum transfer in Compton scattering process are very small, so that atomic electrons cannot be viewed as free electrons anymore. In the low-energy and low-momentum transfer region (correspond to small scattering angle θ), only a small percentage of bound electrons in atomic or molecular systems are activated in the Compton scattering process. Therefore, the FEA results, in which all electrons are treated as free and activated, would tremendously overestimate the angular distribution of Compton scattering process.

For the DDCS of Compton scattering process, the theoretical and experimental results are presented in Figure 5. This figure gives the results of Cu, Sn and Pb elements. It is worth noting that for the DDCS, the FEA result becomes singular at the Compton energy ω_C , while it becomes zero at other energies. This is due to the Dirac delta function $\delta(\omega_f - \omega_C)$ in Equation (10). For this reason, it is not that valuable to plot the FEA result, what we need to focus are the IA and SM predictions. In this figure, subfigures (a), (b) and (c) correspond to the following cases: (a). Compton scattering for Pb atom at $\omega_i = 279.2$ keV and $\theta = 135^\circ$; (b). Compton scattering for K-shell electrons of Sn atom at $\omega_i = 279.2$ keV and $\theta = 115^\circ$; (c). Compton scattering for K-shell electrons of Cu atom at $\omega_i = 59.5$ keV and $\theta = 125^\circ$. The subfigures (a) and (b) display the Compton peak region, while the subfigure (c) presents the spectrum outside the Compton peak. In the subfigure (a), the SM result is calculated by Bergstrom et al. [54], the RIA result is given by Qiao et al. [42], and experimental measurements are given by Rullhusen and Schumacher [83]. In the subfigures (b) and (c), the theoretical SM results are given through combined works of Bergstrom et al. and Gavrilina [28,63], the RIA result is given by Bergstrom et al. [28], and the experimental measurements are given by Basavaraju et al. [84] and Manninen et al. [85], respectively. In subfigure (c), the LET results are calculated by Bergstrom et al. [28]. From these comparisons, some conclusions can be drawn. First, for the DDCS of Compton scattering, the FEA approach becomes deficient and inconvenient, because of the singular behavior in the spectrum. Second, the SM and RIA results are similar in Compton peak region $\omega_f \approx \omega_C$. Both RIA and SM results are consistent with experimental observations in the Compton peak region, when some discrepancies are included. Third, the SM result is largely different from the RIA result outside the Compton peak, due to the infrared rise mentioned in Section 5 (and possible resonant peaks near X-ray characteristic energies, which are not emerged in subfigure (c) (In the SM results, resonant peak behavior often appears in the cases of L and M shell electrons [28,29]. In Figure 5, subfigure (c) corresponds to the Compton scattering with K-shell electrons, so the resonant peaks do not emerge.)). In regions far from the Compton peak, especially the infrared region where final photon energy ω_f is very small, more experimental data are required to test the SM results.

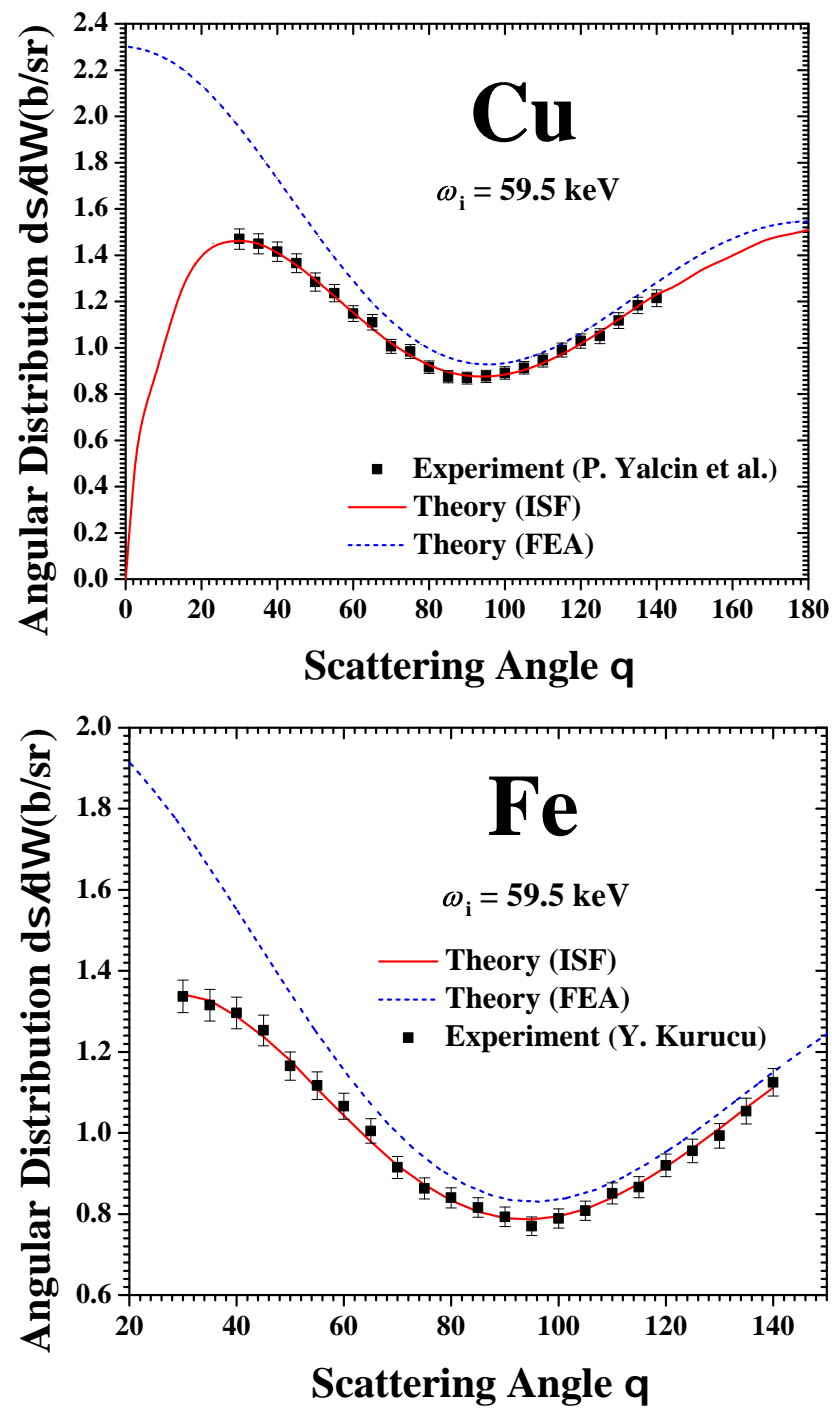


Figure 4. Angular distribution for Compton scattering process at incident photon energy $\omega_i = 59.5$ keV for Fe and Cu. In this figure, the vertical axis labels differential cross sections $d\sigma/d\Omega_f$, and the horizontal axis labels the scattering angle θ . The experimental measurements from reference [80,81] and the theoretical predictions of FEA and ISF approaches [81,82] are plotted in this figure.

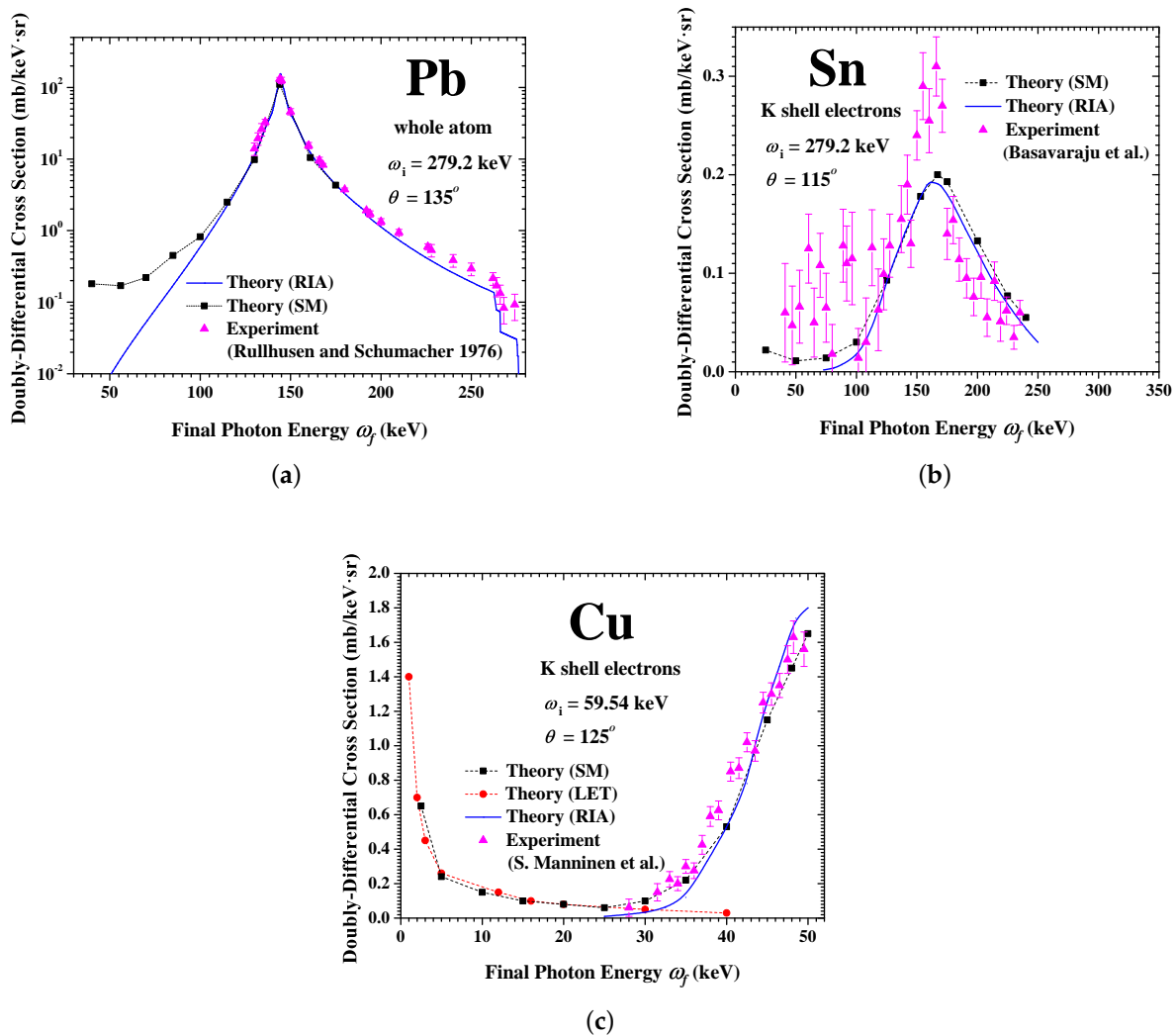


Figure 5. DDCCS of Compton scattering for Cu and Pb elements. In this figure, the vertical axis labels the DDCCS $d\sigma/d\Omega_f d\omega_f$, and the horizontal axis labels the final photon energy ω_f . The subfigures (a–c) correspond to the following cases: (a). Compton scattering for Pb atom at $\omega_i = 279.2$ keV and $\theta = 135^\circ$; (b). Compton scattering for K-shell electrons of Sn atom at $\omega_i = 279.2$ keV and $\theta = 115^\circ$; (c). Compton scattering for K-shell electrons of Cu atom at $\omega_i = 59.5$ keV and $\theta = 125^\circ$. The experimental measurements are given by references [83–85]. The theoretical predictions from RIA and SM approaches are given by Qiao et al. and Bergstrom et al. [28,42,54].

Since RIA result is reliable and consistent with experimental observations in the Compton peak region $\omega_f \approx \omega_C$, we can safely use Compton profile $J(p_z)$ in IA approach to tackle Compton scattering in peak region. In recent decades, much research has emerged to study Compton profiles using the theoretical IA approach combined with experimental measurements near Compton peak [5,7,9]. In experiments, the Compton profiles for atomic or molecular systems can be exacted from experimental data via equation

$$\left[J(p_z) = \iint \rho(\mathbf{p}) dp_x dp_y \right]_{\text{exp}} = \frac{\left(\frac{d^2\sigma}{d\Omega_f d\omega_f} \right)_{\text{exp}}}{Y^{\text{IA}}} \quad (45)$$

Here, $(d^2\sigma/d\Omega_f d\omega_f)_{\text{exp}}$ is the experimental measured DDCCS of Compton scattering. Experimental studies for Compton profile have attracted huge interest in recent years [5,53,86]. Furthermore, there are other quantities similar to the conventional Comp-

ton profile $J(p_z) = \iint \rho(\mathbf{p}) dp_x dp_y$ discussed above. For example, if the incident photon beams are polarized, the differential cross-section is connected with the magnetic Compton profile $[J(p_z)]_{\text{mag}} = \iint [\rho^\uparrow(\mathbf{p}) - \rho^\downarrow(\mathbf{p})] dp_x dp_y$ [87–91], where $\rho^\uparrow(\mathbf{p})$ and $\rho^\downarrow(\mathbf{p})$ are the spin polarized electron momentum densities. Other kinds of Compton profiles, such as the directional Compton profile obtained by setting z axis along different crystallographic axes, are also widely studied in recent years [5,92,93]. Limited to the scope of the present work, we only focus ourselves on the conventional Compton profile $J(p_z)$ defined in Equation (17). Other kinds of Compton profiles are not discussed in detail. More information on various kinds of Compton profiles can be found in references [5,87].

7. Database and Applications

In recent decades, Compton scattering had been extensively applied into many branches of science, including atomic [29], molecular, condensed matter [5–9], astrophysical [94], nuclear and elementary particle physics [47,95,96]. A lot of experimental and theoretical investigations concerning X-rays and gamma-rays cannot be carried on without the help of Compton scattering [36,79,97]. As discussed in Sections 3 and 4, Compton scattering is a powerful tool to study momentum distribution for bound electron in atomic, molecular and condensed matter systems [3–5], both for theoretical and experimental studies. With the help of Compton profile and Compton scattering experiments, electron correlations, Fermi surfaces and band structures in materials can be investigated [6–9]. The Compton profiles are also closely related to the positron annihilation angular correlation spectra [98]. Furthermore, the development of modern gamma-ray spectrometer and imaging devices also benefits a lot from the Compton scattering [99–102].

In recent years, many databases on Compton scattering have already been built up. The most common quantities in tabulations and databases are Compton profile $J(p_z)$, incoherent scattering function $SF(\omega_i, \theta)$, and total cross-section σ (In the theoretical calculations on scattering function $SF(\omega_i, \theta)$ and total cross-section σ , contributions from Compton scattering and Raman scattering cannot be fully distinguished [29]. In numerical tabulations, the contributions from these two processes are summed over to give a total result. In the high energy region, the Compton scattering process is dominant compared with the Raman scattering.). For engineering or industrial applications, the data of differential cross sections $d^2\sigma/d\omega_f d\Omega_f$ and $d\sigma/d\Omega_f$ in Compton scattering can be easily achieved from the tabulation of Compton profile and scattering function (using Equations (3) and (4)). The most widely used database on Compton profile $J(p_z)$ over past years was given by F. Biggs et al. in 1975, in which a complete study on atomic Compton profile for elements ($1 \leq Z \leq 102$) was presented [24]. In Biggs's work, the nonrelativistic Hartree–Fock theory was used to calculate Compton profiles for light elements ($1 \leq Z \leq 36$) and the relativistic Dirac–Hartree–Fock theory was used to calculate Compton profiles for heavy elements ($36 \leq Z \leq 102$). On the scattering function $SF(\omega_i, \theta)$, J. H. Hubbell et al. provided extensive and widely available tabulations for elements ($1 \leq Z \leq 100$) based on Equation (39) in 1975, with ground state wavefunctions calculated by several methods [27]. Later, Kahane gave refined calculations using RIA approach and Dirac–Hartree–Fock ground state wavefunctions for all elements ($1 \leq Z \leq 110$) in 1998 [56]. For the total cross-section σ , J. H. Hubbell et al. also gave tabulations for elements ($1 \leq Z \leq 100$) in their early work in 1975 [27]. The up-to-date tabulations on total cross-section σ are provided by EPDL and NIST databases, which combine the theoretical and experimental data [103,104].

8. Summary

Throughout this paper, we give an overview of the theoretical approaches on the ab initio calculation for Compton scattering with bound electrons in atomic or molecular systems. In this work, we focus on the basic ideas and main results for several approaches. The advantages, validity ranges, and applications of each approach are also briefly explained. These approaches are free electron approximation (FEA), impulse approximation (IA), incoherent scattering factor / incoherent scattering function approximation (ISF), scattering

matrix (SM). Limited to the scope of this work, other approaches and applications are not discussed here, and there are many important works we have not mentioned in this work. We hope that this work would be helpful to theoreticians and experimentalists, especially for those who work on interdisciplinary branches of science with the help of Compton scattering.

Author Contributions: Writing—original draft preparation, C.-K.Q.; writing—review and editing, J.-W.W. and L.C.; project administration, C.-K.Q.; funding acquisition, C.-K.Q. and L.C. All authors have read and agreed to the published version of the manuscript.

Funding: This work was supported by the Scientific Research Foundation of Chongqing University of Technology (Grants No. 2020ZDZ027 and No. 2019ZD21), and the Natural Science Foundation of Chongqing (Grant No. 2020CCZ036).

Institutional Review Board Statement: Not applicable.

Informed Consent Statement: Not applicable.

Data Availability Statement: Not applicable.

Acknowledgments: The authors should also thank to the great efforts from all around the world during the pandemic period of COVID-19.

Conflicts of Interest: The authors declare no conflict of interest.

Abbreviations

The following abbreviations are used in this manuscript:

DDCS	Doubly differential Cross-Section
DHF	Dirac-Hartree Fork
FEA	Free Electron Approximation
HF	Hartree Fork
IA	Impulse Approximation
NRIA	Nonrelativistic Impulse Approximation
RIA	Relativistic Impulse Approximation
ISF	Incoherent Scattering Function/Incoherent Scattering Factor
SM	Scattering Matrix
LET	Low-Energy Theorem

References

1. Compton, A.H. A Quantum Theory of the Scattering of X-rays by Light Elements. *Phys. Rev.* **1923**, *21*, 483–502. [[CrossRef](#)]
2. Compton, A.H. The Spectrum of Scattered X-rays. *Phys. Rev.* **1923**, *22*, 409–413. [[CrossRef](#)]
3. Cooper, M.J. Compton scattering and electron momentum distributions. *Adv. Phys.* **1971**, *20*, 453–491. [[CrossRef](#)]
4. Cooper, M.J. Compton scattering and electron momentum determination. *Rep. Prog. Phys.* **1985**, *48*, 415–481. [[CrossRef](#)]
5. Cooper, M.J. Compton scattering and the study of electron momentum density distributions. *Radiat. Phys. Chem.* **1997**, *50*, 63–76. [[CrossRef](#)]
6. Kubo, Y. Electron correlation effects on Compton profiles of copper in the GW approximation. *J. Phys. Chem. Solids* **2005**, *66*, 2202–2206. [[CrossRef](#)]
7. Rathor, A.; Sharma, V.; Heda, N.L.; Sharma, Y.; Ahuja, B.L. Compton profiles and band structure calculations of IV-VI layered compounds GeS and GeSe. *Radiat. Phys. Chem.* **2008**, *77*, 391–400. [[CrossRef](#)]
8. Wang, Y.J.; Lin, H.; Barbiellini, B.; Mijnders, P.E.; Kaprzyk, S.; Markiewicz, R.S.; Bansil, A. Proposal to determine the Fermi-surface topology of a doped iron-based superconductor using bulk-sensitive Fourier-transform Compton scattering. *Phys. Rev. B* **2010**, *81*, 092501. [[CrossRef](#)]
9. Pisani, C.; Itou, M.; Sakurai, Y.; Yamaki, R.; Ito, M.; Erba, A.; Maschio, L. Evidence of instantaneous electron correlation from Compton profiles of crystalline silicon. *Phys. Chem. Chem. Phys.* **2011**, *13*, 933–936. [[CrossRef](#)] [[PubMed](#)]
10. Klein, O.; Nishina, Y. Über die Streuung von Strahlung durch freie Elektronen nach der neuen relativistischen Quantendynamik von Dirac. *Z. Phys.* **1929**, *52*, 853–868. [[CrossRef](#)]
11. Sakurai, J.J. *Advanced Quantum Mechanics*; Addison-Wesley: New York, NY, USA, 1967.
12. Dumond, J.W.M. Compton Modified Line Structure and its Relation to the Electron Theory of Solid Bodies. *Phys. Rev.* **1929**, *33*, 643–658. [[CrossRef](#)]
13. Dumond, J.W.M. Breadth of Compton Modified Line. *Phys. Rev.* **1930**, *36*, 146–147. [[CrossRef](#)]

14. Dumond, J.W.M. The Linear Momenta of Electrons in Atoms and in Solid Bodies as Revealed by X-ray Scattering. *Rev. Mod. Phys.* **1933**, *5*, 1–33. [[CrossRef](#)]
15. Eisenberger, P.; Platzman, P.M. Compton Scattering of X rays from Bound Electrons. *Phys. Rev. A* **1970**, *2*, 415–423. [[CrossRef](#)]
16. Currat, R.; DeCicco, P.D.; Weiss, R.J. Impulse Approximation in Compton Scattering. *Phys. Rev. B* **1971**, *4*, 4256–4261. [[CrossRef](#)]
17. Eisenberger, P.; Reed, W.A. Gamma-Ray Compton Scattering: Experimental Compton Profiles for He, N₂, Ar, and Kr. *Phys. Rev. A* **1972**, *5*, 2085–2094. [[CrossRef](#)]
18. Eisenberger, P.; Reed, W.A. Relationship of the relativistic Compton cross section to the electron's velocity distribution. *Phys. Rev. B* **1974**, *9*, 3237–3241. [[CrossRef](#)]
19. Ribberfors, R. Relationship of the relativistic Compton cross section to the momentum distribution of bound electron states. *Phys. Rev. B* **1975**, *12*, 2067–2074. [[CrossRef](#)]
20. Ribberfors, R. Relationship of the relativistic Compton cross section to the momentum distribution of bound electron states—II. Effects of anisotropy and polarization. *Phys. Rev. B* **1975**, *12*, 3136–3141. [[CrossRef](#)]
21. Ribberfors, R.; Berggren, K.-F. Incoherent-x-ray-scattering functions and cross sections $(d\sigma/d\Omega)_{incoh}$ by means of a pocket calculator. *Phys. Rev. A* **1982**, *26*, 3325–3333. [[CrossRef](#)]
22. Ribberfors, R. X-ray incoherent scattering total cross sections and energy-absorption cross sections by means of simple calculation routines. *Phys. Rev. A* **1983**, *27*, 3061–3070.; Erratum in: *Phys. Rev. A* **1983**, *28*, 2551. [[CrossRef](#)]
23. Holm, P.; Ribberfors, R. First correction to the nonrelativistic Compton cross section in the impulse approximation. *Phys. Rev. A* **1989**, *40*, 6251–6259. [[CrossRef](#)]
24. Biggs, F.; Mendelsohn, L.B.; Mann, J.B. Hartree-Fock Compton Profiles for the Elements. *At. Data Nucl. Data Table* **1975**, *16*, 201–309. [[CrossRef](#)]
25. Waller, I.; Hartee, D.R. On the intensity of total scattering of X-rays. *Proc. R. Soc. London Ser. A* **1929**, *124*, 119–142. [[CrossRef](#)]
26. Freeman, A.J. A study of the Compton scattering of X-rays, Ne, Cu⁺, Cu and Zn. *Acta Cryst.* **1959**, *12*, 274–279. [[CrossRef](#)]
27. Hubbell, J.H.; Veigele, W.J.; Briggs, E.A.; Brown, R.T.; Cromer, D.T.; Howerton, R.J. Atomic form factors, incoherent scattering functions, and photon scattering cross sections. *J. Phys. Chem. Ref. Data* **1975**, *4*, 471–538.; Erratum in: *J. Phys. Chem. Ref. Data* **1977**, *6*, 615. [[CrossRef](#)]
28. Bergstrom, P.M.; Surić, T.; Pisk, K.; Pratt, R.H. Compton scattering of photons from bound electrons: Full relativistic independent-particle-approximation calculations. *Phys. Rev. A* **1993**, *48*, 1134–1162. [[CrossRef](#)] [[PubMed](#)]
29. Bergstrom, P.M.; Pratt, R.H. An overview of the theories used in Compton Scattering Calculations. *Radiat. Phys. Chem.* **1997**, *50*, 3–29. [[CrossRef](#)]
30. Kaplan, I.G.; Barbiellini, B.; Bansil, A. Compton scattering beyond the impulse approximation. *Phys. Rev. B* **2003**, *68*, 235104. [[CrossRef](#)]
31. Surić, T. Compton scattering beyond impulse approximation: Correlation, nonlocal-exchange and dynamic effects. *Radiat. Phys. Chem.* **2006**, *75*, 1646–1650. [[CrossRef](#)]
32. Pratt, R.H.; LaJohn, L.A.; Florescu, V.; Surić, T.; Chatterjee, B.K.; Roy, S.C. Compton scattering revisited. *Radiat. Phys. Chem.* **2010**, *79*, 124–131. [[CrossRef](#)]
33. Drukarev, E.G.; Mikhailov, A.I.; Mikhailov, I.A. Low-energy K-shell Compton scattering. *Phys. Rev. A* **2010**, *82*, 023404.; Erratum in: *Phys. Rev. A* **2011**, *83*, 029901. [[CrossRef](#)]
34. Drukarev, E.G.; Mikhailov, A.I. *High Energy Atomic Physics*; Springer International Publishing: Basel, Switzerland 2016.
35. Sparks, C.J. Inelastic resonance emission of X-rays: Anomalous scattering associated with anomalous dispersion. *Phys. Rev. Lett.* **1974**, *33*, 262–265. [[CrossRef](#)]
36. Kane, P.P. Experimental studies of inelastic X-ray and gamma ray scattering. *Radiat. Phys. Chem.* **1997**, *50*, 31–62. [[CrossRef](#)]
37. Jung, M.; Dunford, R.W.; Gemmell, D.S.; Kanter, E.P.; Krässig, B.; LeBrun, T.W.; Southworth, S.H.; Young, L.; Carney, J.P.J.; LaJohn, L.; et al. Manifestations of Nonlocal Exchange, Correlation, and Dynamic Effects in X-Ray Scattering. *Phys. Rev. Lett.* **1998**, *81*, 1596–1599. [[CrossRef](#)]
38. Carney, J.P.J.; Pratt, R.H. Constructing adequate predictions for photon-atom scattering: A composite approach. *Phys. Rev. A* **2000**, *62*, 012705. [[CrossRef](#)]
39. Roy, S.C.; Pratt, R.H. Need for further inelastic scattering measurements at X-ray energies *Radiat. Phys. Chem.* **2004**, *69*, 193–197. [[CrossRef](#)]
40. Chatterjee, B.K.; LaJohn, L.A.; Roy, S.C. Investigations on compton scattering: New directions. *Radiat. Phys. Chem.* **2006**, *75*, 2165–2173. [[CrossRef](#)]
41. Kircher, M. Kinematically complete experimental study of Compton scattering at helium atoms near the threshold. *Nat. Phys.* **2020**, *16*, 756–760. [[CrossRef](#)]
42. Qiao, C.-K.; Chi, H.-C.; Zhang, L.; Gu, P.; Liu, C.-P.; Tang, C.-J.; Lin, S.-T.; Huang, K.-N. Relativistic Impulse Approximation in Compton Scattering. *J. Phys. B: At. Mol. Opt. Phys.* **2020**, *53*, 075002. [[CrossRef](#)]
43. Qiao, C.-K.; Chi, H.-C.; Lin, S.-T.; Gu, P.; Liu, S.-K.; Tang, C.-J. Compton Scattering Spectrum for Si and Ge Systems. *J. Phys. G Nucl. Part. Phys.* **2020**, *47*, 045202. [[CrossRef](#)]
44. Thomson, J.J. *Conduction of Electricity through Gases*; Cambridge University Press: Cambridge, UK, 1906.
45. Namito, Y.; Ban, S.; Hirayama, H. Implementation of the Doppler broadening of a Compton-scattered photon into the EGS4 code. *Nucl. Instrum. Meth. A* **1994**, *349*, 489–494. [[CrossRef](#)]

46. Ordóñez, C.E.; Bolozdynya, A.; Chang, W. Doppler broadening of energy spectra in Compton cameras. *IEEE Nucl. Sci. Symp. Conf. Rec.* **1997**, *2*, 1361–1365. [[CrossRef](#)]
47. Brusa, D.; Stutz, G.; Riveros, J.A.; Fernández-Varea, J.M.; Salvat, F. Fast sampling algorithm for the simulation of photon Compton scattering. *Nucl. Instrum. Meth. A* **1996**, *379*, 167–175. [[CrossRef](#)]
48. Mendelsohn, L.B.; Biggs, F.; Mann, J.B. Relativistic hartree-fock compton profiles for the rare gases and lead. *Chem. Phys. Lett.* **1974**, *26*, 521–524. [[CrossRef](#)]
49. Dyall, K.G.; Grant, I.P.; Johnson, C.T.; Parpia, F.A.; Plummer, E.P. GRASP: A general-purpose relativistic atomic structure program. *Comput. Phys. Commun.* **1989**, *55*, 425–456. [[CrossRef](#)]
50. Bauer, G.E.W.; Schneider, J.R. Density-functional theory of the compton profiles of beryllium metal. *Solid State Commun.* **1986**, *47*, 673–676. [[CrossRef](#)]
51. Bauer, G.E.W.; Schneider, J.R. Density-Functional Theory of the Compton Profile Anisotropy of Copper Metal. *Z. Phys. B Condens. Mat.* **1983**, *54*, 17–24. [[CrossRef](#)]
52. Parr, R.G.; Rupnik, K.; Ghosh, S.K. Phase-Space Approach to the Density-Functional Calculation of Compton Profiles of Atoms and Molecules. *Phys. Rev. Lett.* **1986**, *56*, 1555–1558. [[CrossRef](#)] [[PubMed](#)]
53. Aguiar, J.C.; Mitnik, D.; Rocco, H.O.D. Electron momentum density and Compton profile by a semi-empirical approach. *J. Phys. Chem. Solids* **2015**, *83*, 64–69. [[CrossRef](#)]
54. Bergstrom, P.M.; Surić, T.; Pisk, K.; Pratt, R.H. Some preliminary calculations of whole atom Compton scattering of unpolarized photons. *Nucl. Instrum. Meth. B* **1992**, *71*, 1–6. [[CrossRef](#)]
55. Kaliman, Z.; Pisk, K.; Pratt, R.H. Compton scattering from positronium and validity of the impulse approximation. *Phys. Rev. A* **2011**, *83*, 053406. [[CrossRef](#)]
56. Kahane, S. Relativistic Dirac-Hartree-Fock Photon Incoherent Scattering Functions. *At. Data Nucl. Data Tables* **1998**, *68*, 323–347. [[CrossRef](#)]
57. Kane, P.P. Inelastic scattering of X-rays and gamma rays. *Radiat. Phys. Chem.* **2006**, *75*, 2195–2205. [[CrossRef](#)]
58. Schnaidt, F. Über das kontinuierliche und diskontinuierliche Comptonspektrum bei Wasserstoff. *Ann. Phys.* **1934**, *21*, 89–112. [[CrossRef](#)]
59. Gummel, A.; Lax, M. Thermal capture of electrons in silicon. *Ann. Phys.* **1957**, *2*, 28–56. [[CrossRef](#)]
60. Schumacher, M.; Smend, F.; Borchert, I. Incoherent scattering of gamma rays by inner-shell electrons. *J. Phys. B At. Mol. Phys.* **1975**, *8*, 1428–1439. [[CrossRef](#)]
61. Gavrilă, M. Compton Scattering by K-Shell Electrons. I. Nonrelativistic Theory with Retardation. *Phys. Rev. A* **1972**, *6*, 1348–1359. [[CrossRef](#)]
62. Gavrilă, M. Compton Scattering by K-Shell Electrons. II. Nonrelativistic Dipole Approximation. *Phys. Rev. A* **1972**, *6*, 1360–1367. [[CrossRef](#)]
63. Gavrilă, M. Numerical results for nonrelativistic Compton scattering of photons by K-shell electrons in the dipole approximation. *Rev. Roum. Phys.* **1974**, *19*, 473–487.
64. Gavrilă, M.; Tugulea, M.N. Compton scattering by L-shell electrons—II. *Rev. Roum. Phys.* **1975**, *20*, 209–230.
65. Whittingham, I.B. Incoherent scattering of gamma rays in heavy atoms. *J. Phys. A Gen. Phys.* **1971**, *4*, 21–37. [[CrossRef](#)]
66. Whittingham, I.B. Compton Scattering of 279.1 and 661.6 keV photons by K-shell electrons. *Aust. J. Phys.* **1981**, *34*, 163–184. [[CrossRef](#)]
67. Surić, T.; Bergstrom, P.M.; Pisk, K.; Pratt, R.H. Compton scattering of photons by inner-shell electrons. *Phys. Rev. Lett.* **1991**, *67*, 189–192. [[CrossRef](#)] [[PubMed](#)]
68. Surić, T. Compton scattering from bound electrons: Comparisons of the impulse approximation with exact IPA calculation. *Nucl. Instrum. Meth. A* **1992**, *314*, 240–243. [[CrossRef](#)]
69. Kramers, H.A.; Heisenberg, W. Über die Streuung von Strahlung durch Atome. *Z. Phys.* **1925**, *31*, 681–708. [[CrossRef](#)]
70. Wailer, I. Über eine verallgemeinerte Streuungsformel. *Z. Phys.* **1928**, *51*, 213–231. [[CrossRef](#)]
71. Wailer, I. Die Streuung kurzwelliger Strahlung durch Atome nach der Diracschen Strahlungstheorie. *Z. Phys.* **1929**, *58*, 75–94. [[CrossRef](#)]
72. Peskin, M.E.; Schroeder, D.V. *An Introduction to Quantum Field Theory*; Westview Press: Chicago, IL, USA, 1995.
73. Rosenberg, L.; Zhou, F. Soft-photon approximation for bound-state Compton scattering. *Phys. Rev. A* **1991**, *44*, 7283–7289. [[CrossRef](#)]
74. Florescu, V.; Gavrilă, M. Soft-photon emission in extreme-relativistic Compton scattering by K-shell electrons and connection to photoeffect. *Radiat. Phys. Chem.* **2000**, *59*, 127–136. [[CrossRef](#)]
75. Chatterjee, B.K.; Roy, S.C.; Surić, T.; Lajohn, L.A.; Pratt, R.H. Asymmetry and the shift of the Compton profile. *Nucl. Instrum. Meth. A* **2007**, *580*, 22–24. [[CrossRef](#)]
76. Hopersky, A.N.; Nadolinsky, A.M.; Novikov, S.A. Intershell correlations in Compton photon scattering by an atom. *Phys. Rev. A* **2010**, *82*, 042710. [[CrossRef](#)]
77. Hopersky, A.N.; Nadolinsky, A.M.; Novikov, S.A. Compton scattering of two x-ray photons by an atom. *Phys. Rev. A* **2015**, *92*, 052709. [[CrossRef](#)]
78. Hopersky, A.N.; Nadolinsky, A.M.; Novikov, S.A. Rayleigh scattering of two X-ray photons by an atom. *Phys. Rev. A* **2016**, *93*, 052701. [[CrossRef](#)]

79. Kane, P.P. Inelastic scattering of X-rays and gamma rays by inner shell electrons. *Phys. Rep.* **1992**, *218*, 67–139. [[CrossRef](#)]
80. Kurucu, Y. Incoherent scattering cross-sections for elements with $23 \leq Z \leq 51$ at 59.5 keV photon energy. *J. Electron Spectrosc.* **2005**, *142*, 39–43. [[CrossRef](#)]
81. Yalcin, P.; Ekinici, N.; Kurucu, Y. Incoherent scattering of ^{241}Am gamma photons. *Spectrochim. Acta. B* **2002**, *57*, 791–796. [[CrossRef](#)]
82. Wang, X.J.; Miguel, B.; Seuntjens, J.; Fernández-Varea, J.M. On the relativistic impulse approximation for the calculation of Compton scattering cross sections and photon interaction coefficients used in kV dosimetry. *Phys. Med. Biol.* **2020**, *65*, 125010. [[CrossRef](#)]
83. Rullhusen, P.; Schumacher, M. Cross section profiles for Compton scattering of 279.2 keV photons by copper, tin and lead. *J. Phys. B Atom. Molec. Phys.* **1976**, *9*, 2435–2446. [[CrossRef](#)]
84. Basavaraju, G.; Kane, P.P.; George, S.M. Compton scattering of 279.2-keV γ rays by K-shell electrons. *Phys. Rev. A* **1987**, *36*, 655–664. [[CrossRef](#)]
85. Manninen, S.; Hämäläinen, K.; Graeffe, J. Inelastic photon scattering from K-shell electrons of Cu and Zr. *Phys. Rev. B* **1990**, *41*, 1224–1226. [[CrossRef](#)] [[PubMed](#)]
86. Suortti, P.; Buslaps, T.; Fajardo, P.; Honkima, V.; Meinander, T. Scanning X-ray spectrometer for high-resolution Compton profile measurements at ESRF. *J. Synchrotron Rad.* **1999**, *6*, 69–80. [[CrossRef](#)]
87. Sakurai, H.; Itoh, F.; Ota, M.; Takano, K.; Liu, X.; Oike, H.; Kawat, H. Development of measuring magnetic Compton profiles by grazing incidence geometry. *J. Phys. Chem. Solids* **2004**, *65*, 2083–2088. [[CrossRef](#)]
88. Benea, D.; Minár, J.; Ebert, H.; Chioncel, L. Magnetic Compton profiles of disordered $\text{Fe}_{0.5}\text{Ni}_{0.5}$ and ordered FeNi alloys. *Phys. Rev. B* **2018**, *97*, 144408. [[CrossRef](#)]
89. Agui, A.; Harako, A.; Shibayama, A.; Haishi, K.; Tsuji, N.; Liu, X.; Ma, C.; Sakurai, H. Temperature dependence of the microscopic magnetization process of $\text{Tb}_{12}\text{Co}_{88}$ using magnetic Compton scattering. *J. Magn. Magn. Mater.* **2019**, *484*, 207–211. [[CrossRef](#)]
90. Dashora, A.; Suthar, M.; Kumar, K.; Choudhary, R.J.; Phase, D.M.; Sakurai, H.; Tsuji, N.; Sakurai, Y.; Ahuja, B.L. Study of magnetism in Fe doped CoCr_2O_4 using magnetic Compton scattering and first-principles computations. *J. Alloy. Compd.* **2020**, *824*, 153883. [[CrossRef](#)]
91. James, A.D.N.; Sekania, M.; Dugdale, S.B.; Chioncel, L. Magnetic Compton profiles of Ni beyond the one-particle picture: Numerically exact and perturbative solvers of dynamical mean-field theory. *Phys. Rev. B* **2021**, *103*, 115144. [[CrossRef](#)]
92. Apell, S.P.; Cabrera-Trujillo, R.; Oddershede, J.; Trickey, S.B.; Sabin, J.R. Effect of shape on molecular directional Compton profiles. *J. Mol. Struct.* **2000**, *527*, 157–163. [[CrossRef](#)]
93. Koizumi, A.; Kubo, Y.; Yamamoto, E.; Haga, Y.; Sakurai, Y. Electronic Structure in Heavy Fermion Compound UPd_2Al_3 through Directional Compton Profile Measurement. *J. Phys. Soc. Jap.* **2019**, *88*, 034714. [[CrossRef](#)]
94. Porter, T.A.; Moskalenko, I.V.; Strong, A.W.; Orlando, E.; Bouchet, L. Inverse Compton Origin of the Hard X-ray and Soft Gamma-Ray Emission from the Galactic Ridge. *Astrophys. J.* **2008**, *682*, 400–407. [[CrossRef](#)]
95. Ji, X. Deeply virtual Compton scattering. *Phys. Rev. D* **1997**, *55*, 7114–7125. [[CrossRef](#)]
96. Ramanathan, K.; Kavner, A.; Chavarria, A.E.; Privitera, P.; Amidei, D.; Chou, T.-L.; Matalon, A.; Thomas, R.; Estrada, J.; Tiffenberg, J.; et al. Measurement of low energy ionization signals from Compton scattering in a charge-coupled device dark matter detector. *Phys. Rev. D* **2017**, *96*, 042002. [[CrossRef](#)]
97. Brown, J.M.C.; Dimmock, M.R.; Gillam, J.E.; Paganin, D.M. A low energy bound atomic electron Compton scattering model for Geant4. *Nucl. Instrum. Meth. B* **2014**, *338*, 77–88. [[CrossRef](#)]
98. Dugdale, S.B. Probing the Fermi surface by positron annihilation and Compton scattering. *Low Temp. Phys.* **2014**, *40*, 328–338. [[CrossRef](#)]
99. Takada, A. Development of an advanced Compton camera with gaseous TPC and scintillator. *Nucl. Instrum. Meth. A* **2005**, *546*, 258–262. [[CrossRef](#)]
100. Mihailescu, L.; Vetter, K.M.; Burks, M.T.; Hull, E.L.; Craig, W.W. SPEIR: A Ge Compton camera. *Nucl. Instrum. Meth. A* **2007**, *570*, 89–100. [[CrossRef](#)]
101. Chiu, J.-L. The upcoming balloon campaign of the Compton Spectrometer and Imager (COSI). *Nucl. Instrum. Meth. A* **2015**, *784*, 359–363. [[CrossRef](#)]
102. Phuoc, K.T.; Corde, S.; Thauray, C.; Malka, V.; Tafzi, A.; Goddet, J.P.; Shah, R.C.; Sebban, S.; Rousse, A. All-optical Compton gamma-ray source. *Nat. Photonics* **2012**, *6*, 308–311. [[CrossRef](#)]
103. Cullen, D.E.; Hubbell, J.H.; Kissel, L. *EPDL97: The Evaluated Photon Data Library 97 Version*; Lawrence Livermore National Laboratory Report UCRL-50400; Lawrence Livermore National Lab.: Livermore, CA, USA, 1997; Volume 6, pp. 1–28; doi:10.2172/295438. [[CrossRef](#)]
104. Berger, M.J.; Hubbell, J.H.; Seltzer, S.M.; Chang, J.; Coursey, J.S.; Sukumar, R.; Zucker, D.S.; Olsen, K. *XCOM: Photon Cross Sections Database*; NIST Standard Reference Database 8 (XGAM); Center for Radiation Research: Washington, DC, USA, 2010; doi:10.18434/T48G6X. [[CrossRef](#)]